A comparison of the hydrodynamic characteristics of surface runoff generated by flash floods in geologically different areas of the Bohemian Massif (crystalline rocks) and the western Carpathians (flysch)

Vilém SPÁLOVSKÝ [a] [*], Stanislav RUMAN [a], Milan TRIZNA [b]

Abstract

The geological environment is undoubtedly one of the basic factors that influence the formation of surface runoff. The extent to which this factor can also affect the hydrodynamic characteristics of flash floods, which is also indirectly associated with flood risk, is the main topic of this study. In two geologically different areas of the Bohemian Massif (crystalline rocks predominate) and the western Carpathians (flysch rocks predominate), a total of 40 watersheds characterised by sharing a certain hydrological analogy were selected (20 watersheds from the Massif and 20 from the Flysch zone). In each of these watersheds, 1-year, 10-year and 100-year flash flood return periods were constructed using the two-dimensional hydrodynamic model Iber. The outputs from this model included raster datasets of areas, depths, and flow velocities during inundations. Subsequently, these rasters were analysed and compared with an emphasis on differences within the individual geological study areas. The outputs showed clear differences in the individual hydrodynamic characteristics (e.g. the average inundation area during Q_{100} was 29.07% larger in the Flysch than in the Massif). Overall, the Flysch zone appeared to be far riskier in terms of flash floods than in the case of the Bohemian Massif.

Key words: Flash floods, 2D hydrodynamic modelling, factors affecting floods, flood risk, Flysch zone, Bohemian Massif, Iber model, Czech Republic

1. Introduction

According to European Commission (2006), we can describe floods as natural phenomena that causes the "temporary covering by water of land not normally covered by water". There are several possibilities for how such water coverage can occur and how the floods themselves are classified. In Europe, according to the HANZE (2017) database, we most often encounter riverine floods, i.e. floods that affect larger watercourses, mainly during periods of long-duration (> 1 day) rainfall or intense snow cover melt. Furthermore, we encounter so-called flash floods, which, in contrast, mainly affect small watercourses after short (< 1 day) and heavy torrential rains. In coastal areas, we encounter coastal floods, which most often occur because of storm surges.

In general, we can say that the floods in Europe are some of the most dangerous natural hazards that occur in the area (Gvoždíková and Müller, 2017; Kundzewicz et al., 2018). There have been several occurrences of this phenomenon in recent decades, with serious negative effects on the health, lives, and property of the inhabitants (Blöschl et al., 2020; Paprotny et al., 2018; UNDRR, 2019). The outlook for the future is also unfavourable. Winsemius et al. (2015) assume that climate change will lead to a significant increase in global flood risk, which cannot be avoided in Europe. This calls for more mitigation and adaptation measures and an overall better understanding of this phenomenon to reduce economic and especially human losses. This study strives to become a part of this conversation.

[a] Department of Physical Geography and Geoecology, Faculty of Science, University of Ostrava, Czech Republic (*corresponding author: V. Spálovský, e-mail: *vilem.spalovsky@osu.cz*)

[b] Department of Physical Geography and Geoinformatics, Faculty of Natural Science, Comenius University, Bratislava, Slovakia

As many authors (e.g. Diakakis et al., 2020; Fragoso et al., 2012; Gaume et al., 2009; Sene, 2013) have shown, especially dangerous floods are caused by short-term (< 1 day), high-intensity precipitation events, predominantly of convective origin, that arise locally in small areas (< 100 km^2), i.e. flash floods (Bryndal, 2015; Marchi et al., 2010). In addition, this type of flood is problematic in terms of its extreme difficulty in forecasting (Vincendon et al., 2011). This is based on the accuracy of the measured data in real-time and the accuracy and temporal and spatial resolution of meteorological models and their forecast lead times, as well as the accuracy of hydrological models (Hapuarachchi et al., 2011).

At first glance, it is obvious that a combination of individual forecast components may introduce many errors and uncertainties that are not easy to address, although several techniques and innovations have been developed in recent years that significantly improve the forecasting of flash floods (Berkhahn et al., 2019; Mosavi et al., 2018; Zanchetta and Coulibaly, 2020). It is still not possible to predict all events with sufficient accuracy, especially events in small ungauged watersheds (Hapuarachchi et al., 2011; Ntelekos et al., 2006). Unfortunately, these small watersheds may also occur in heavily urbanised areas, where flash floods occur almost without warning and may have catastrophic consequences (Hardy et al., 2016).

To prevent or at least reduce these consequences, a variety of measures may help (e.g. Kreibich et al., 2015; Krzhizhanovskaya et al., 2011; Poussin et al., 2015). In addition to technical measures and various warning systems, flood hazard mapping and flood risk mapping play very important roles. Mapping enables us to identify critical areas for floods, pre-assess the level of risk in these areas and then make efforts to reduce the consequences of possible floods. According to Directive 2007/60/EC, a preliminary flood risk assessment is required for each EU member state for all types of floods, including flash floods. As the literature has indicated, several different methods are used for this purpose worldwide (e.g. Kandilioti and Makropoulos, 2011; Li et al., 2012; Wang et al., 2011). Nevertheless, only a few methods are used in conjunction with flash floods.

One of the few examples is the research of Zeleňáková et al. (2015), which described the preliminary assessment of flood risk from flash floods based on the so-called Critical Point Method (CPM). This method was derived by Drbal et al. (2009) after a series of catastrophic flash floods in 2009 in the Czech Republic. The CPM cannot be used as a stand-alone tool for the preliminary assessment of flood risks, however, as it only detects areas prone to flash floods based on selected physical-geographic characteristics and the presence of built-up areas (Štěpánková et al., 2017). By supplementing the CPM with a suitable risk analysis, we may obtain a relatively good method for the preliminary assessment of flash flood risks, even on a national scale, which fully complies with the requirements of Directive 2007/60/EC. In our study, the CPM was used as a tool for the selection of research sites, and it is described more specifically in the Materials and Methods section.

A crucial part of our work is hydrodynamic modelling. In recent decades, this modelling has become an integral part of flood risk management, and its outputs serve as tools for decision makers. There have been an increasing number of studies that use hydrodynamic models to determine flood risk (Baky et al., 2019; Dinh et al., 2012; Masood

and Kuniyoshi, 2011), even in small ungauged watersheds (Li et al., 2019; Vojtek and Vojteková, 2016). Using hydrodynamic models, the hydrodynamic characteristics can be simulated, i.e. the area and depth of inundation and the velocity of flow. Using these characteristics, the degree of flood hazard is determined. Flood hazard is a fundamental component of the resulting flood risk. According to Wisner et al. (2004), we can simply formulate the resulting flood risk as a combination of vulnerability and flood hazard: Risk = Vulnerability × Hazard. Coupled hydrological models (or rainfall-runoff models) can also be used for more complex analyses. These models are coupled with hydrodynamic models and provide information about the shape of the flood wave (i.e. the flood hydrograph). This approach is used mainly in large-scale modelling (Paiva et al., 2013; Xia et al., 2019) but also in areas of ungauged watersheds (Li et al., 2019; Vojtek et al., 2019).

The propagation of floods can be affected by several factors (see Section 2.2), including the geological environment of the affected area, which may also contribute to some extent (Chen et al., 2020; Gutiérrez et al., 2014; Norbiato et al., 2009). We observe that methodologies for preliminary flood risk assessment are often applied nationwide, regardless of the various geological environments: we do not know to what extent these environments affect the resulting hydrodynamic characteristics of flash floods. In our study, we focus specifically on flash floods and demonstrate how geological settings can affect these characteristics and thus the resulting flood risk.

The main aim of this study is to respond to the following questions, which have not been discussed thus far:

- What is the resulting hydrodynamic behaviour of watercourses below the critical points?;

- Is there a real flood risk below all critical points and, if so, under what N-year return period (N-year flood scenario)?; and

- How can this behaviour differ regarding different quasi-homogeneous geological areas? This is the most important question.

For example, in the conditions of the Czech Republic, where in one part of the country (Bohemian Massif), there are mostly resistant crystalline rocks (but with aquiferous fractures), and in other parts, there are poorly permeable sedimentary rocks of the Flysch belt (western Carpathians). Much of the literature (Kourgialas and Karatzas, 2011; O'Connor et al., 2002; Spellman et al., 2019) has emphasised the fact that the geological environment may significantly contribute to the formation of riverine floods and thus form one of the basic factors that influence these events. We know that it can also affect flash floods in highly permeable rocks, i.e. in karsts, where a specific type of flash flood occurs (Bonacci et al., 2006; Gutiérrez et al., 2014; Zanon et al., 2010).

What has not been much described in the literature, however, is to what extent this factor can affect the nature of flash floods in strongly impermeable rocks such as flysch rocks. Not only in the case of the CPM but also in other similar methods, this geological factor is often omitted and not calculated. For this reason, we consider it desirable to find answers to the abovementioned questions so that in the future, we can make the CPM (and possibly other methods) a more credible and robust basis for preliminary flood risk assessment. We also aim to fill gaps in the understanding of this phenomenon.

2. Theoretical background

2.1 Hydrodynamic modelling

As outlined earlier, hydrodynamic models are a valuable aid in estimating the extent and nature of floods. The core elements of these models are mathematical-physical governing equations, which are based on the physical laws of conservation of mass, momentum, and energy. Individual modelling software usually employs two control equations: the continuity equation and the momentum equation (Liu, 2018). These equations can be used in various modifications, and it is only up to the modelling software what set of equations it offers. Simplified forms of the equations may give less accurate results; however, models using them may be stable and have shorter computational times (Brunner, 2016). Several modelling software programs, both commercial and open source, are used worldwide. Teng et al. (2017), in their review, present more than 30 well-known hydrodynamic modelling software programs that allow flood inundations to be modelled.

Individual models may differ further in terms of dimensionality. Commonly applied hydrodynamic models in flood simulations are one-dimensional (1D) (Mark et al., 2004; Masood and Takeuchi, 2012), dominantly two-dimensional (2D) (Ernst et al., 2010; Mihu-Pintilie et al., 2019) or coupled 1D / 2D (Patel et al., 2017; Seyoum et al., 2012). With the 1D approach, the movement of water is simulated in only one direction, perpendicular to the individual cross sections. The main advantage of this approach is shorter computational time and less demand for topographic data (Costabile et al., 2015). Its suitability is limited mainly to simple watercourses and events in which no overflow occurs (Patel et al., 2017; Srinivas et al., 2009). In contrast, the 2D approach allows one to simulate the flow of water in two directions within a predefined computer network. The significant advantage of this approach is that it can simulate the flow of water around various obstacles, such as buildings, which is exactly what is needed in flood inundation modelling (Neal et al., 2010; Schubert and Sanders, 2012; Petroselli et al., 2019). Another possibility is a combination of the above-mentioned approaches, where the 1D approach is used for the stream channel and the 2D approach is used for the adjacent floodplain, as was done, for example, by Patel et al. (2017).

Information on the peak discharge of a flood event with a certain return period serves as the basic input data for hydrodynamic flood modelling. These peak discharges are either determined based on time series from the measured data, can be calculated on the basis of regional empirical formulas or can be estimated using hydrological models. As an example, we present the work of Petroselli et al. (2019), who compare the regional method according to Dub (1957) with the outputs of hydrological models and describe how the individual approaches affect the resulting hydrodynamic modelling. Petroselli et al. (2019) also point to the development of the digital elevation model (DEM), which is another essential component that is necessary for hydrodynamic modelling and whose quality can significantly affect the results. A DEM is a continuous representation of bare earth, on which surface runoff is generated and subsequently transported during the hydrodynamic modelling process. DEM is an integral part of the model's governing mechanisms. Many authors (e.g. Bates et al., 1998; Baugh et al., 2013; Jarihani et al., 2015) report that DEM accuracy is the factor that can most significantly affect the results of hydrodynamic models. For detailed modelling, which is used, for example, in the case of small watercourses, it is necessary to use very accurate, LiDAR-based (Light Detection and Ranging) DEMs with the lowest possible spatial resolution (Vaze et al., 2010). As further reported by Vaze et al. (2010), a very good resolution for these purposes is approximately 1 m (DEM cell size 1 × 1 m).

2.2 Flash flood propagation and influencing factors

The propagation of a flash flood in the natural environment is influenced by several factors with which we can work to a certain extent in the modelling environment. Aside from meteorological factors, which are undoubtedly the main triggering mechanism of flash floods, physical-geographical and anthropogenic factors play important roles. As Hewlett and Hibbert (1967) stated for small watercourses, these are mainly the average slope of the watershed, land use and the pedological-geological conditions of the area. The average slope of the watershed affects the flow velocity. If the slope of the watershed increases, then the average runoff rate increases and the time of concentration decreases. This is reflected in the watershed by a faster increase in the peak flow, which results in larger peak discharges (Gray, 1964; Subramanya, 2008). Land use characteristics mainly affect the infiltration capacity of soils and create a retarding effect for overland flow (Subramanya, 2008). Changes in land use may significantly cause a change in the flood flow regime (Brath et al., 2006). Some studies have reported that changes in land use may modify the average annual flow by 10% (Huisman et al., 2009; Li and Wang, 2009; Ruman et al., 2020).

Even geological characteristics, however, can be crucial in terms of the formation of the resulting flood event. To a certain extent, they influence the previously described physical-geographic factors and thus have a significant indirect effect on flood wave propagation. The geological setting of a given area affects, for example, the height of the erosion base level of a given watercourse (Kukal, 2005). Furthermore, the geological setting affects the morphology of the watercourse (width, depth, sinusoid, etc.) and the entire river network, which is due to the resistance of rocks and the properties of river sediments (Schumm, 1960; Schumm, 1985). These morphological factors determine the efficiency of a river basin to attenuate flood waves (Gray, 1964). Lithology also affects roughness conditions as well as the amount and properties of river sediments. It also plays a unique role in soil-forming substrates, that affects pedogenetic factors (e.g. infiltration). From this point of view, the most important role is played by superficial geology (Ruman et al., 2020). Direct effects are also notable due to the formation of a hydrogeological environment, which can have a significant retention capacity (Lauber et al., 2014; Spellman et al., 2019).

3. Material and Methods

3.1 Critical points method

Because torrential rains in Europe usually affect a very small area in a short period of time, their spatial and temporal prediction is considerably complicated. Also problematic is determining the intensity of torrential rain, which governs the issuance of warning information by the flood forecasting service, despite the relatively dense network of precipitation stations. Therefore, the prior identification and evaluation

of critical points where there is a potential risk of flash floods is approached to ensure the elimination of negative consequences. For this purpose, the so-called critical points method is used in the Czech Republic as a suitable "national" strategy to reduce the risk of torrential rain (Novák and Tomek, 2015; Drbal et al., 2009).

Drbal et al. (2009) developed a nationwide survey for this purpose, the output of which is a point layer showing the critical points of inflow of storm water into an urban area with municipalities, and an area layer of the contributing watershed belonging to each point.

The procedure for locating individual critical points follows Drbal et al. (2009) and Štěpánková et al. (2017) and is as follows:

First, it was necessary to generate flow accumulation paths using a digital terrain model (10 × 10 m) and GIS tools (ArcHydro). The first set of critical points was identified in areas where these paths intersect with the boundaries of urban areas (for example, see Fig. 1). The individual critical points were also assigned an appropriate contributing area, for which the following physical-geographic characteristics were calculated: size of the contributing area, average slope, proportion of arable land area and the so-called critical condition index (CI).

The critical condition index was calculated according to the following formula:

$$C_I = A \cdot P \cdot (w_1 \cdot m + w_2 \cdot PAL + w_3 \cdot CN_{II}) \qquad (1)$$

where C_I is the index of critical conditions; A is the relative value of the size of the contributing area (with respect to a maximum considered size of 10 km^2) [-]; P is the relative value of the total one-day precipitation with a repetition period of 100 years for the territory of the Czech Republic (with respect to a maximum of 285.7 mm) [-]; w is the weight vector [1.48876; 3.09204, 0.467171]; m is the average slope of contributing area [%]; PAL is the proportion of arable land in the area [%]; and CN_{II} is the value of CN_{II} for the territory of the Czech Republic, which represents characteristics of the contributing area in consideration of run-off.
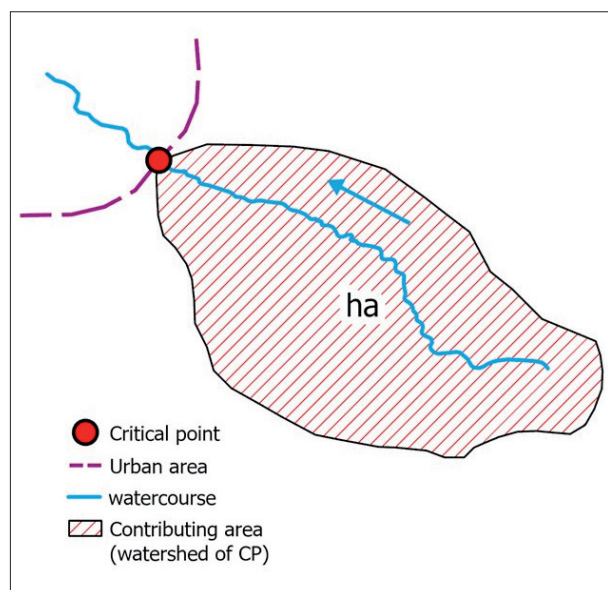
Fig. 1: Example of a critical point and its contributing area. Source: authors' compilation

The next step was the selection of critical points based on the criteria that were determined based on observations after flood events in the Czech Republic in 2009 and are as follows:

i.   The size of the contributing area is in the range of 0.3–10 km^2;

ii. The average slope of the contributing area ≥ 3.5%;

iii. The proportion of arable land area ≥ 40%; and

iv. The critical condition index ≥ 1.85.

The results of this method included the determination of 9,261 geolocated critical points and their contributing areas throughout the Czech Republic. We used these points and areas in our research to determine and localise the study areas (Drbal et al., 2009; Štěpánková et al., 2017).

3.2 Selection of study areas

Immediately below each critical point, a certain area exists where a flood can have a negative effect on the life, health, and property of the inhabitants. These areas are exactly the goal of our study. Given that a large number of critical points were identified, research, in terms of time, personnel and finances, could not be conducted in all these locations. Therefore, it was necessary to select a small but representative sample, which was subsequently investigated.

From the national dataset of all critical points, 20 points from a geological area in the Bohemian Massif and 20 points from a geological area in the Flysch zone were selected (for an overview of characteristics: see Fig. 5 in Results section, below; for localisation: see Fig. 2). The selection was made using a geoinformation system in such a way that the individual contributing areas of the critical points (watersheds of individual critical points, for example see Fig. 1) had similar characteristics regarding area size, slope and share of arable land to the greatest extent possible (see Fig. 5, below). This was achieved by multiple point filtering using the structured query language. The individual points, which differed significantly from the rest of the dataset, were gradually erased until only 20 points remained in each of the geological areas. The resulting points were thus as similar as possible in all observed characteristics. This reduced the contributions from other factors affecting the character of surface runoff and, conversely, emphasised the geological environment.

For each critical point, we subsequently determined N-year return periods (1-yr, 10-yr and 100-yr), which served as basic input data for two-dimensional hydrodynamic models.

3.3 Determination of values of individual N-year return periods

The calculation of single N-year return periods was carried out by using an hydrological analogy method. In the individual geological areas in the Massif and Flysch, we selected a group of stream gauging stations with the smallest possible contributing area so that they corresponded as closely as possible to our examined catchment area of critical points. The area of selected gauged catchments was within the range of 4.1–28.9 km^2. Subsequently, freely available data (N-year return periods) were obtained from the Czech Hydrometeorological Institute (hereinafter CHMI). CHMI is computes N-year return periods from annual maximal flows and/or proxy data of historical floods (where available) and uses three various statistical distributions. The selection of a particular distribution is based on expert estimates. In the next step, the average of these N-year flows ($\varnothing Q_N$) was calculated, and the average area of the watershed
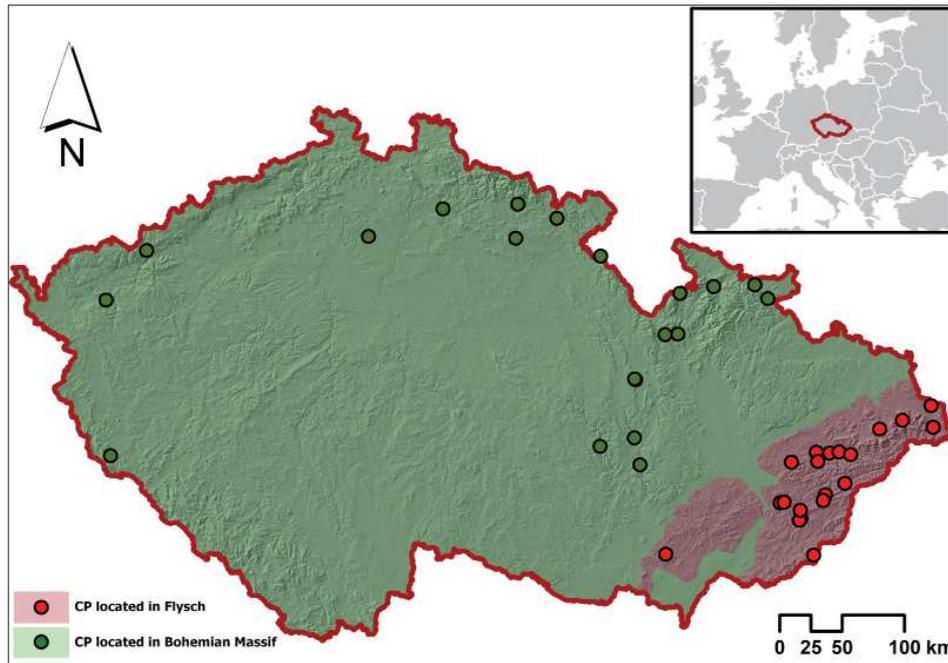
Fig. 2: Selected critical points (CP) within the Czech Republic and their distribution according to the relevant geological area
Sources: Eurostat, EU-DEM, GeoCR500, and authors' compilation

($\varnothing A$) belonging to the gauging stations was calculated. By dividing $\varnothing Q_N$ by $\varnothing A$, we obtained a coefficient by which we continued to multiply the areas of critical point watersheds (A_i), based on which we obtained missing information about the required N-year discharges in our critical point catchments.

The values of individual $\varnothing Q_N$ and $\varnothing A$ for the Massif and Flysch are presented in the Results section in Table 2, and the calculation is schematised by the following equation:

$$Q_{N_i} = A_i \cdot \frac{\varnothing Q_N}{\varnothing A} \qquad (2)$$

3.4 Process of hydrodynamic modelling

For modelling, we selected the freely available Iber software version 2.5.2., which, according to Pinos and Timble (2019), shows very good results in mountain basin areas, and this corresponded exactly to our research areas. In addition, it turned out that the calculation of the Iber model was much more stable for our research areas than, for example, the HEC-RAS model, where there were problems with model stabilisation. The Iber model can automatically adjust the computational time (even less than 0.1 s) to satisfy the Courant condition, which makes it a very good and stable tool that is more suitable for our conditions. This model has also appeared very often in the literature in connection with two-dimensional hydrodynamic (2D HD) modelling in flash flood conditions (e.g. Bodoque et al., 2016; Garrote et al., 2016; Ruiz-Villanueva et al., 2014a).

As reported by Bladé et al. (2014), the Iber model is a two-dimensional numerical model used to simulate turbulent free surface unsteady flow and other environmental processes in stream hydraulics. For our case, i.e. modelling the area and depth of inundation and flow velocities, we used a hydrodynamic module, which uses the finite volume technique to solve the 2D shallow water equations (2D Saint-Venant Equations).

The governing equations represent a set of partial differential equations that describe the conservation of mass and momentum in the two horizontal directions as shown below (Bladé et al., 2014; Hydraulic Reference Manual Iber v1.0, 2014):

$$\frac{\partial h}{\partial t} + \frac{\partial h U_x}{\partial x} + \frac{\partial h U_y}{\partial y} = M_S; \qquad (3)$$

$$\frac{\partial h U_x}{\partial t} + \frac{\partial h U_x^2}{\partial x} + \frac{\partial h U_x U_y}{\partial y} = \qquad (4)$$

$$= -gh\frac{\partial Z_s}{\partial x} + \frac{\tau_{s,x}}{\rho} - \frac{\tau_{b,x}}{\rho} - \frac{g}{\rho} + \frac{h^2}{2}\frac{\partial \rho}{\partial x} +$$

$$+ 2\omega \sin \lambda U_y + \frac{\partial h \tau_{xx}^e}{\partial x} + \frac{\partial h \tau_{xy}^e}{\partial y} + M_X;$$

$$\frac{\partial h U_y}{\partial t} + \frac{\partial h U_x U_y}{\partial x} + \frac{\partial h U_y^2}{\partial y} = \qquad (5)$$

$$= -gh\frac{\partial Z_s}{\partial y} + \frac{\tau_{s,y}}{\rho} - \frac{\tau_{b,y}}{\rho} - \frac{g}{\rho} + \frac{h^2}{2}\frac{\partial \rho}{\partial y} -$$

$$- 2\omega \sin \lambda U_x + \frac{\partial h \tau_{xy}^e}{\partial x} + \frac{\partial h \tau_{yy}^e}{\partial y} + M_Y$$

where t is time; x and y represent the directions of the Cartesian coordinate system used; h is water depth; U_x and U_y are depth-average horizontal velocities; g is the acceleration of gravity; Z_s is free surface elevation; τ_s is the friction on the free surface due to friction produced by wind; τ_b is the friction at the bottom; ρ is the density of the water; ω is the angular velocity of the Earth's rotation; λ represents the latitude of the studied point; τ_{xx}^e, τ_{xy}^e and τ_{yy}^e are the

effective horizontal shear stresses; and M_s, M_x and M_y are the terms of mass source and momentum, which are used to model precipitation, infiltration and drainage.

The model was developed downstream of all localities (critical points). Equal lengths of watercourses were established at 300 m. The mean slope of the watercourses in the Bohemian Massif was 0.036 m/m with a standard deviation of 0.017. For the Flysch streams, these values were 0.031 and 0.011 for the mean and standard derivation, respectively. As the morphology of the floodplain is also important in flood hazard studies, we calculated the mean width of the floodplain, where the floodplain was considered an area equal to the borders of the Q_{100} inundation area. The mean value was calculated in ArcGIS Pro, creating stream centreline, and automatically creating a cross section every 10 metres. Then, the mean value and standard deviation were calculated.

3.5 Topographic data

The basic topography is represented using a digital elevation model (DEM) DMR 5G obtained from the Czech Office for Surveying, Mapping and Cadastre. This DEM was created by laser scanning for the entire territory of the Czech Republic and has a high resolution of 1×1 m with a mean height error of up to 0.18 m (ČUZK, 2021). Due to the lack of information regarding the shape of cross-sections, we decided to leave the bathymetry of watercourses unchanged without making any corrections. We only filtered out transverse obstacles such as bridges and culverts, so that the stream channel allows the flow of Q_{100} at the location of the obstacle. The deviation of bathymetry can introduce small uncertainties into the results of the 2D HD model (for more details, see Section 5: Discussion, below); however, the topographic conditions were the same for all research sites, and the results of the comparison of outputs were not affected to any large extent.

For the needs of our research, it was still necessary to add volumes of buildings to the DEM, so that the flow around the individual buildings during inundation was resolved. For this purpose, we used building polygons from the Open Street Map project (OpenStreetMap®, 2019), to which we then assigned a uniform height using a GIS application and converted them to raster data. We continued to merge the raster volumes of the buildings with the DEM, thus creating a pseudo digital model of the surface, i.e. the relief + building model but without vegetation cover (an example is shown in Fig. 3). We used the pseudo digital surface model created in this way as input topographic data, based on which an irregular triangular computational network was generated in the Iber model (length of triangle edge $\leq$ 1 m).

3.6 Roughness coefficient

For the model to calculate an important input parameter, bed friction (τ_b), it was necessary to know the value of the so-called bed friction coefficient (C_f). For this purpose, the model used the Iber Manning equation in the following form (Hydraulic Reference Manual Iber v1.0, 2014):

$$C_f = g \frac{n^2}{h^{\frac{1}{3}}} \qquad (6)$$

where g is the gravity acceleration; h is the depth and n is the Manning roughness coefficient that needs to be entered manually. For our case, we entered a uniform value of 0.06 for all research sites, so that the same conditions were
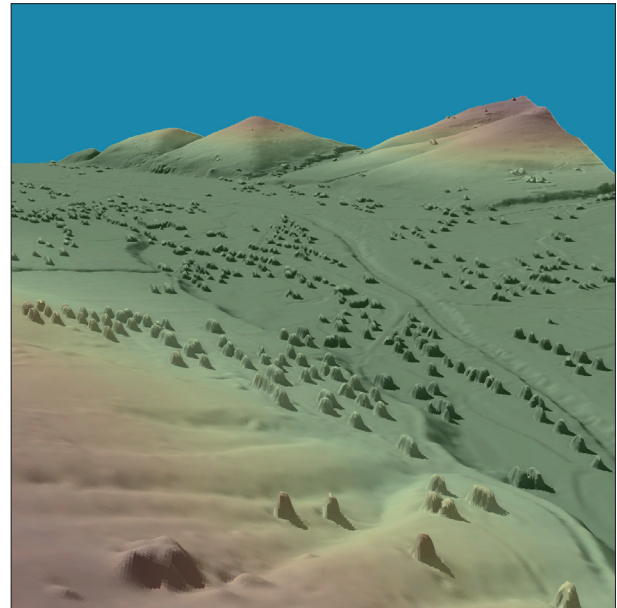
Fig. 3: Example of pseudo digital surface model used in this work as input topography to the 2D HD models
Sources: authors' compilation based on Open Street Map data and DMR 5G

maintained. We estimated this value based on a manual by Arcement and Schneider (1989) with regard to the similarity of individual research sites.

3.7 Other parameters in the model

Other settings of the 2D hydrodynamic model included the selection of a numerical scheme, where we chose the 2nd-order scheme, which is slower to calculate and less stable, but the outputs are much more accurate. Initial conditions were considered without prior water contribution (initial depth = 0 m). The overall settings are presented in Table 1. With this model setting, depth and flow velocity rasters at a 1×1 m resolution were calculated for each N-year scenario (Q_1, Q_{10} and Q_{100}) for each research area.

3.7 Flood risk assessment – endangered area

To determine whether there is a potential occurrence of flood risk below certain critical points and possibly how this occurrence differs in the Flysch and Massif, we created a very simple method of so-called endangered areas. The endangered area represents the area of buildings in which the inhabitants may reside or where their property may be, and at the same time this area intersects the area of inundation of a certain N-year scenario. During a particular flood scenario, a certain risk may occur in such an endangered area. In this method, however, we did not quantify the degree of risk: we only determined in a binary metric whether a potential risk may occur and, if so, to what extent.

With the settings of the model presented in the previous steps, rasters of depths and water flow velocities at a resolution of 1×1 m were calculated for individual N-year scenarios (Q_1, Q_{10} and Q_{100}) for each research area (a total of 240 raster outputs). The models differed only in input topography and input flow values. For completeness, the area of flow velocities greater than 1 m.s^{-1} and the area of depths greater than 1 m were added. This represents areas where more significant manifestations of flash floods occur. All post-processing with raster data was performed in the software application ArcGIS Pro.

Iber model settings	Choice
Module	2D hydrodynamic module
Computational network	Irregular triangular network with a resolution of 1×1 m
Topography	Modified DMR 5G (1×1 m)
Roughness	Based on Manning roughness coefficient with value of 0.06
Numerical Scheme	2nd-order
Inlet	Total discharge of individual N-year return periods (in the form of steady flow)
Initial conditions	Depth (0 m)
Upper boundary condition	Total discharge (one value for a given N-year return period)
Result exportation	Rasters of water depths and velocities in a resolution of 1×1 m (Nearest-neighbour interpolation)

Tab. 1: Overview of the resulting settings of the Iber model in version 2.5.2. for 2D HD modelling in this study Source: authors' compilation

4. Results

Table 2 presents the average N-year discharges and average contributing area derived from gauging stations. For completeness, we added information on the average annual rainfall and the average slope in the gauging station watersheds. Table 3 presents the average values of discharges obtained using the hydrological analogy method in individual geological areas and their differences within individual return periods. This average was calculated based on the resulting input flow data, presented in Table 2. At first glance, there are already differences in the hydrological behaviour of small streams between the Flysch and Massif. The streams below CP in the Flysch zone show 36.03% higher values of discharges at Q_1, 37.84% at Q_{10} and 32.97% at Q_{100}.

Under these conditions, the differences in the output rasters of depths and water flow velocities are also obvious. This is evidenced by a graphical representation in the form of boxplots (see Fig. 4) and representation in the form of a table with values of absolute and percentage differences of individual outputs, for individual modelled N-year return periods: see Table 4.

	$\varnothing Q_1$ [$m^3.s^{-1}$)]	$\varnothing Q_{10}$ [$m^3.s^{-1}$)]	$\varnothing Q_{100}$ [$m^3.s^{-1}$)]	$\varnothing A$ [km^2]	$\varnothing$**Annual Rainfall** [mm]	$\varnothing$**Slope** [%]
Bohemian Massif	4.73 ± 2.16	17.30 ± 5.63	40.26 ± 12.25	18.28 ± 6.61	979 ± 143	13.8 ± 2.4
Flysch Zone	7.15 ± 3.35	26.94 ± 10.22	58.12 ± 17.97	17.89 ± 6.44	$1,020 \pm 109$	15.9 ± 3.4

Tab. 2: Average N-year discharge and average contributing area in individual geological areas obtained from gauging stations. Sources: Input data from the Czech Hydrometeorological Institute; authors' calculations Note: "±" denotes standard deviation (number to the right of this symbol)

Table 4 shows that the average inundation area of flash floods is larger in the Flysch in all examined N-year return periods. At Q_1 it is 31.74% larger; at Q_{10} it is 34.7% larger; and at Q_{100} it is 29.07% larger than those in the Bohemian Massif. These values are like the magnitude of differences in average discharges shown in Table 2. There are also larger average water depths in the Flysch which increase with increasing recurrence interval, where the largest percentage difference is observed in Q_{100} (16.11%), followed by Q_{10} (14.4%) and Q_1 (7.88%). In contrast, the Massif has slightly higher average flow velocities, which are 8.62% higher at Q_1, 2.8% higher at Q_{10} and 4.94% higher at Q_{100}. A clear pattern was not found when comparing differences in the magnitude of return periods and values of average flow velocities. The situation is diametrically different, however, if we examine only average areas where the flow velocity exceeds 1 m.s^{-1}. These areas are characterised by increased flood extremities and may have an increased flood risk. Such areas dominate in the Flysch, where the largest differences are observed at Q_{100} (20.08%) and Q_{10} (20.63%). During Q_1, they predominate by only 6.18%. Large fluctuations are represented by the average areas of depths greater than 1 m, where the Flysch prevails only in the case of extreme flow Q_{100} by 30.94%. During Q_{10}, the average areas of depths greater than 1 m already prevail in the Massif, namely, by 7.9%, and during Q_1, they prevail by 33.04% (see further discussion in Section 5, below).

The mean width of the floodplain (see Fig. 5) was 29.51 m in Flysch, with a standard deviation of 14.01. Lower values were reported in the Massif: 22.07 and 10.53 for the mean and standard deviation, respectively.

The interquartile range (IQR) as a measure of dispersion was higher in the Flysch watershed in all scenarios for the area of inundation and the area of depths > 1 m, than in the Massif. For the water depth, Flysch watersheds had a higher IQR for Q_1 and Q_{10} but a lower IQR for Q_{100} than

	$\varnothing Q_1$ [$m^3.s^{-1}$)]	$\varnothing Q_{10}$ [$m^3.s^{-1}$)]	$\varnothing Q_{100}$ [$m^3.s^{-1}$)]
Massif	0.40	1.45	3.37
Flysch	0.62	2.33	5.03
Diff.	0.22	0.88	1.66
Diff. (%)	36.03	37.84	32.97

Tab. 3: The resulting average discharges of individual N-year return periods obtained by the hydrological analogy method. Source: authors' calculations Note: Diff. and Diff. (%) were computed between Q_N of Flysch and Massif. Q_N denotes the discharge with certain N-year return period

the Massif watershed. Dispersion was higher in the Massif for all scenarios of flow velocity and for scenarios Q_1 and Q_{10} for an area of velocities > 1 m.s^{-1} (Fig. 4).

Table 5 describes the outputs from the endangered area method for scenarios Q_{100} and Q_{10} (at Q_1 the endangered area is negligible). The table shows that the largest endangered area below critical points within our research sites is in the

Flysch zone, both during Q_{100} (almost 57% more) and Q_{10} (almost 71% more). The table also shows the total number of research sites in which at least some unquantified risk is demonstrated using 2D HD models. Most such sites are again in the Flysch, where at Q_{100}, there are 16 areas (in 4 cases, the model did not confirm any flood risk) and at Q_{10} there are 11 areas (in 9 cases, the model did not confirm any flood risk).

		Area of inundation [m^2]	Water depth [m]	Flow velocity [m.s^{-1}]	Area of velocities > 1 m.s^{-1} [m2]	Area of depths > 1 m [m^2]
Q_1	Massif	2,854.60	0.19	0.49	225.50	113.35
	Flysch	4,182.05	0.21	0.45	240.35	85.20
	Diff.	1,327.45	0.02	− 0.04	14.85	− 28.15
	Diff. (%)	31.74	7.88	− 8.62	6.18	− 33.04
Q_{10}	Massif	4,113.75	0.23	0.72	743.85	140.75
	Flysch	6,302.45	0.27	0.70	937.15	130.45
	Diff.	2,188.70	0.04	− 0.02	193.30	− 10.30
	Diff. (%)	34.73	14.40	− 2.80	20.63	− 7.90
Q_{100}	Massif	5,874.25	0.26	0.90	1,427.70	162.80
	Flysch	8,281.45	0.31	0.86	1,786.45	235.75
	Diff.	2,407.20	0.05	− 0.04	358.75	72.95
	Diff. (%)	29.07	16.11	− 4.94	20.08	30.94

Tab. 4: The resulting values of individual hydrodynamic characteristics under different N-year return periods and their comparison within different areas of the Flysch and the Massif. Source: authors' calculations
Note: Differences were computed between Flysch and Massif. Q_N denotes the discharge with certain N-year return period
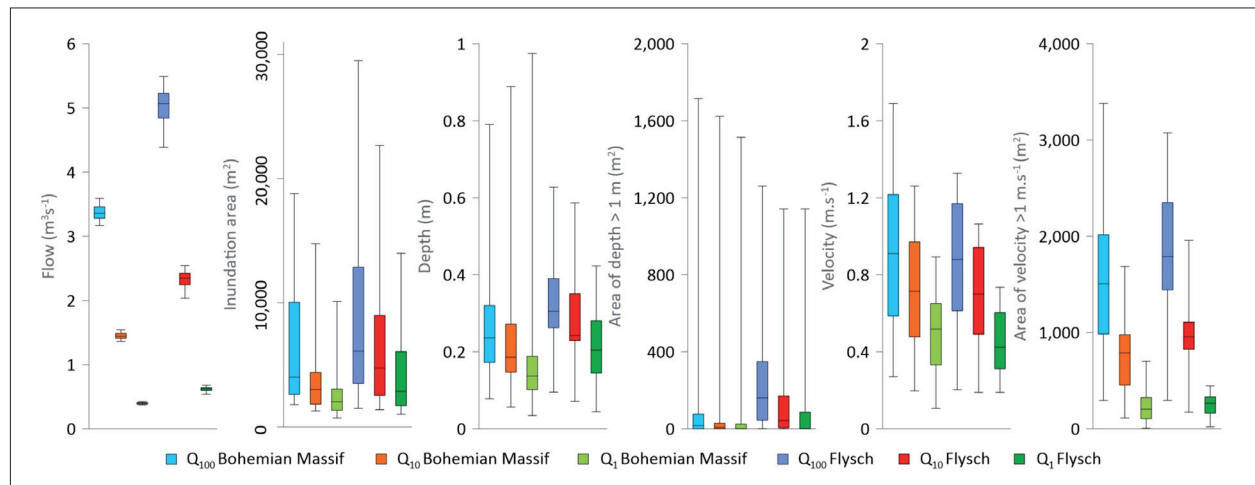
Fig. 4: Hydrodynamic characteristics of flash floods during different flood scenarios in different geological areas of the Flysch and the Massif. Graph whiskers indicate minimum and maximum values. The upper bound of the boxplot indicates Q_3, and the lower bound of the boxplot indicates Q_1. The median is used as a measure of central tendency Source: authors' calculations

	Massif Q_{100}	Flysch Q_{100}	Massif Q_{10}	Flysch Q_{10}
∑ Endangered area [m^2]	7626.34	17534.89 (56.6% larger)	2994.29	10292.8 (70.9% larger)
Number of research sites with potential flood risk (out of 20)	14	16 (12.5% larger)	7	11 (63.6% larger)

Tab. 5: The size of endangered areas (within research sites) and the total number of research sites with a potential occurrence of flood risk in different conditions in the Flysch and Massif
Source: authors' calculations
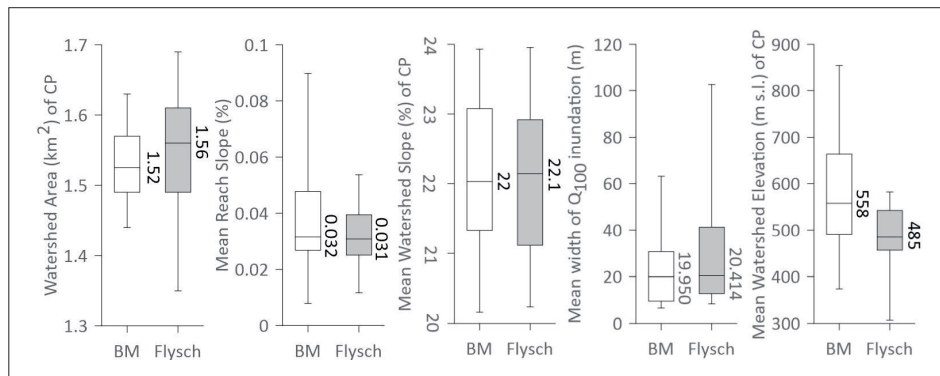
Fig. 5: Comparison of characteristics of selected critical points (respectively their watersheds). For better comparison, added information about mean reach slope and mean width of Q_{100} inundation (downstream of CP)
Source: authors' calculations

5. Discussion

5.1 Hydrodynamic modelling

As part of the methodological procedure, we determined the value of the Manning roughness coefficient based on the manual from Arcement and Schneider (1989). It must be said that in the case of the construction of precise and detailed 2D HD models, it is necessary to further adjust the values selected in this way during the process of calibration and validation of the model using real observed data. An example is the work of Pestana et al. (2013), in which the authors focused on the calibration of the model using the difference between the simulated inundation and the real inundation obtained from remote sensing images (using SAR). In their case, the optimal value of the Manning roughness coefficient was found to be 15% higher than the predetermined value. A more common method is to calibrate the model based on the observed water levels or discharges obtained from gauging stations. A typical example is the work of Smolders et al. (2012), in which the authors used both approaches. In our case, however, such a step could not occur due to the absence of gauging stations at our research sites or the lack of knowledge regarding historical floods. It was not even desirable, however, because our primary purpose was not to create precise 2D HD models, but models that have the closest possible conditions so that we can then evaluate them based on the hydrodynamic behaviour of streams within the different geological areas. Therefore, we applied a uniform value of the Manning roughness coefficient (n = 0.06) in all modelled areas.

Subsequently, we tried to evaluate the uncertainty that can be caused by different roughness values in real conditions. Ruman et al. (2021) also faced a similar problem in their work. They proceeded by choosing a method of repeated modelling with 6 different values of the Manning roughness coefficient (differing by one hundredth) and then determining a range of peak flows at individual roughness values, which differed by up to 40% in total. In our work, we also decided to use repeated modelling with a different value of the Manning roughness coefficient (specifically, n = 0.04), to compare the areas of inundations at different values of n. It turned out that the differences in the inundation areas of the output rasters modelled with a value n = 0.06 and rasters modelled with a value n = 0.04 of the Manning roughness coefficients are within a range of 5%. We believe that this indicates that the influence of Manning values did not change the main results of this study; indeed, the uncertainty in Manning values remains, as noted in previous studies.

Not only hydrodynamic modelling, but also any other environmental modelling is burdened with several uncertainties, and it is necessary to think critically when assessing the results (Beven, 2009). The same is true in our study. In addition to the uncertainties that stem from the lack of model calibration, these also include primarily the uncertainties associated with the digital elevation model. As mentioned by Papaioannou et al. (2016), DEM accuracy plays one of the most important roles in the modelling process. Although we chose the most accurate, commercially used elevation model for the Czech Republic, DMR 5G with a resolution of 1 × 1 m, this model can still be burdened with a mean error of height of up to 0.18 m (ČUZK, 2021). Another limitation of DMR 5G is the method of its construction, i.e. the use of infrared radiation for the detection of individual height points on the relief. Infrared radiation is largely absorbed by water, which can cause deviations in watercourse bathymetry.

Nevertheless, we believe that these deviations are not too large because sensing was performed on clear days with minimal cloud cover; therefore, we assume that water levels in our research streams were not above average and only reached a few cm. During the dry parts of the year, some streams may even be almost free of water; therefore, they do not constitute an obstacle to the passage of infrared radiation. Furthermore, it must be emphasised that our models do not consider the transport of sediments or other floating debris or ice (e.g. tree logs, trash or ice floes). These objects can clog the cross-section in places with obstacles on the watercourse (e.g. under bridges) and thus cause inundation even in places other than those shown in the models. More on this issue was presented, for example, by Ruiz-Villanueva et al. (2014b), who even modelled a situation where the water level increased by several metres due to a clogged cross-section, which our models would not have captured.

In addition, all transverse objects in watercourses (bridges and culverts) were removed from our DEM, which, according to many authors, are the main places that limit water runoff (Pappenberger et al., 2006; Diehl, 1997; Ruiz-Villanueva et al., 2012). All of this can cause some differences between real inundations and those modelled. Importantly, for all our modelled areas, a DEM created under the same conditions was applied, i.e. the individual models were burdened with the same uncertainties; thus, the results of the comparison of outputs are likely not affected to any great degree.

5.2 Discussion of results

We can already observe considerable differences in runoff between the Flysch and the Massif, based on the outputs from the hydrological analogy method (input values of N-year discharges: see Tab. 3). Each watershed examined in this study was not gauged, however. Thus, no observed hydrological data were available, and the flow values for each scenario were calculated from the return period of analogue gauged watersheds within the same geological group. The criteria for the selections of gauged watersheds were the geological formation, watershed area, watershed slope and proportion of arable land. This was indeed a crucial procedure that influenced the results of this study. Although this method is commonly applied (Petroselli et al., 2019), it should be noted, that hydrological behaviour (e.g. return periods) of large (average area is approximately 18 km^2), gauged watersheds are transformed to the behaviour of smaller (average area is approximately 1.5 km^2), ungauged watershed. This simplification was applied due to the limited number of small, gauged watersheds, meaning that both large and small catchments have equal hydrological response, which is certainly not true, especially when connected with geological characteristics. Thus, the differences between the hydraulic characteristics simulated in this study should be considered maximal differences. More methods should be employed, such as rainfall-runoff modelling (Młyński, 2020) or artificial neural networks (Filipova et al., 2022), to calculate the return periods and examine the hydraulic behaviours in two geologically different areas to support the findings in this article.

If we examine the 100-year scenario, then we can say that the discharges are higher in the Flysch, on average by up to 32.9%. The same proportion does not prevail for individual HD characteristics. The percentage difference in the case of the inundation area compared with the inlet discharges decreases slightly, which is, however, reflected in the larger average depths of the inundations in the case of the Flysch. Larger inundation areas and at the same time greater water depths during individual N-year scenarios in the Flysch, nevertheless, significantly increase the value of the wetted perimeter. Due to friction, there is a greater kinetic loss of flowing water in the Flysch zone, which is reflected in lower average flow velocities. Even watercourses in the Massif achieve higher average flow velocities in individual N-year scenarios than in the Flysch zone.

Another reason why the water depth and velocities had opposite behaviours in the same geological areas (in Flysch higher water depths and lower water velocities) can be related to the mean width of the floodplain and slope of the stream (see Fig. 5). The results showed that higher values of the mean floodplain width were found in Flysch than in the Massif (the difference was 25.2%). Thus, the flow is more concentrated in Massif watersheds; therefore, velocities were higher. The width of the floodplain was calculated from the inundation area, however, and it demonstrated a clear connection with the input flows which influenced the results. Thus, more methods of floodplain delineation should be envisaged (Clubb et al., 2017) to confirm this conclusion. Furthermore, a higher stream slope was reported in the Massif watershed (13.89%), which further increases this contradictory behaviour. This situation is, however, diametrically different in the case of areas with velocities larger than 1 m.s^{-1}. In the Flysch, running water (especially during Q_{100} and Q_{10}) is concentrated in a larger stream tube, and areas with flow velocities greater than

1 m.s^{-1} are thus significantly larger than those in Massif. If such a stream tube intersects with a built-up area, its kinetic energy can cause considerable damage and thus significantly increase the potential flood risk. Furthermore, areas with depths greater than 1 m have considerable fluctuation. This fluctuation, however, is because in the case of some research sites, depths greater than 1 m do not appear at all; therefore, the resulting area of depths greater than 1 m may be zero in some cases. Consequently, with decreasing input flow, these "zero" areas increase. This causes the resulting arithmetic mean to be significantly affected by these outliers. A better choice is to use a different measure of central tendency; in our case, we used the median, which in this case is a more reliable statistical representation. The percentage difference of the median of areas with a depth > 1 m is then always greater for the Flysch than for the Massif, as follows: at Q_1 by 50%, at Q_{10} by 85% and at Q_{100} by up to 90%. The medians for all output rasters are presented within the boxplots in Figure 4.

Many authors (e.g. van Alphen et al., 2009; Kreibich et al., 2009; Smith, 1994) have stated that the important parameters affecting flood damage are mainly depth and flow velocity. In addition, if we consider the areas of greatest depths and greatest flow velocities, we can consider the Flysch as a far riskier area in terms of flash floods in individual N-year scenarios than in the Bohemian Massif. This finding is in accordance with the study of Gaal et al. (2012), where the authors examined watersheds with various geological characteristics. As noted by Norbiato et al. (2009), the influence of geology on runoff can be isolated only by comparing catchments with similar rainfall characteristics. The mean values of annual rainfall calculated for the gauged watershed in both geologically different regions from where the return period was scaled to the watershed of critical points were 979 mm in the Bohemian Massif and 1,020 mm in Flysch (4.02% difference; see Tab. 2 for details). Thus, the condition of similarity based on rainfall was fulfilled.

In this study, the dispersion in hydraulic characteristics was documented by IQR (Fig. 4). First, the three discharges (return periods) were developed at the beginning of the modelling. The dispersion was highest in Flysch watersheds. These results can be explained by the higher standard deviation of the watershed area in Flysch (Fig. 5) compared to that in the Massif. Thus, the high dispersion in IQR from the watershed area was transferred to high dispersion in IQR of discharges as they were calculated by the hydrological analogy applying the watershed area (see Equation 2). Second, the dispersion in discharges was transferred to the simulated results of hydraulic characteristics (area of inundation, water depth, flow velocity, area of depths > 1 m and flow velocity). For the area of inundation and area of depths > 1 m, the highest dispersion was found in the Flysch watersheds compared to the Massif watersheds, which agrees with the dispersion of discharges. For the water depth this was true only for scenarios Q_1 and Q_{10}. The Massif had a higher dispersion of water depth for scenario Q_{100}. Dispersion was higher in the Massif for all scenarios of flow velocity and for scenarios Q_1 and Q_{10} for areas of velocities > 1 m.s^{-1} (Fig. 4). These higher values can be explained by the higher values of the standard deviation of the stream slope and higher IQR of the watershed area.

The results continue to show that during the individual peaks of the flood scenarios, the floods in the Flysch are characterised by higher magnitudes (Tab. 3). This can be explained by the reduced permeability of this geological

environment, which subsequently generates a larger amount of surface runoff during floods. This is also demonstrated by Trpkosova et al. (2008), who, from a more hydrogeological point of view, examined the same geological structures with which we worked. Trpkosova et al. (2008) add that the values of the specific groundwater runoff from the Flysch area (in the Beskydy Mountains) can be up to 65% lower than for the Bohemian Massif (in the Jeseník Mountains). They further add that at the time of flood discharges, the specific groundwater runoff in the Flysch is only minimally affected compared to that of the Bohemian Massif, which corresponds to our finding of different runoff behaviours on the surface. The permeability of the geological environment itself thus seems to be an important factor in the formation of floods. This is also demonstrated by the study of Norbiato et al. (2009), where the authors additionally suggest that the analysis of hydrogeological area types can help predict flood response in ungauged watersheds. A similar topic was addressed, for example, by the studies of Chen et al. (2020) and Sharma et al. (2019), which also confirmed a certain role of the geological environment in the formation of surface runoff. In our work, we managed to further expand these findings and show that the geological environment not only affects the runoff response but also affects the hydrodynamic characteristics of floods, even in the case of flash floods. These characteristics then represent the degree of flood hazard, which is the basic input to the calculation of the flood risk itself (Merz et al., 2007; Wisner et al., 2004). Thus, it is obvious that even the resulting flood risk can be affected by different geological environments. The resulting degree of flood risk is the subject of future research.

The literature dealing with the characteristics of flash floods in connection with the geological environment is limited exclusively to karst areas. There are several studies (e.g. Bonacci et al., 2006; Gutiérrez et al., 2014; Zanon et al., 2010, etc.) that describe a specific type of flood in karst areas, which is caused by a highly permeable geological environment. There is a lack of studies dealing with specific floods in other geological areas, however. Based on the results of our work, we perceive the behaviour of floods in the geological area of the Flysch as a kind of counterpoint to karst areas. The different geology of the Flysch area of the Western Carpathians in comparison with the crystalline rocks of the Bohemian Massif, causes obvious differences in the hydrodynamic characteristics of floods; in this respect, the Flysch area and floods, which occur here with a certain specificity, add to the research.

Interesting approach and possible direction of future work would be to increase the amount of critical points applied in this study (20 in both geologic areas) to support our results. However, this extension would also cause reduced similarity of new watersheds of critical points which was defined by three watershed characteristics. In the end, this would cause increase the uncertainty in the comparison.

6. Conclusions

In this study, we focus on observations of the differences in the hydrodynamic characteristics of flash floods in geologically different areas of the Bohemian Massif (crystalline rocks) and the western Carpathians (flysch rocks). We focus our observations on the so-called critical points at which there should be a significant assumption of the occurrence of this phenomenon. In 40 analogous watersheds of critical points (20 from the Massif and 20 from the Flysch), a total of 120 2D HD models were constructed for N-year scenarios of 1-year,

10-year and 100-year flash floods. Based on the comparison of the outputs from these models, we draw the following conclusions and suggestions.

The differences in the individual hydrodynamic characteristics within the two different geological areas of the Flysch and the Massif have been clearly demonstrated. In all individual N-year scenarios, the flash floods in the Flysch zone have a larger average inundation area and a larger average depth during these inundations. Only the average flow velocities during the inundations are slightly higher in the Bohemian Massif than in the Flysch zone probably because of the higher reach slope in the Massif. If we take into account the areas with flow velocities greater than 1 m.s^{-1}, however, which we consider to be much riskier, then again, floods in the Flysch zone clearly prevail.

Overall, flash floods in the Flysch area appear to be riskier in all observed N-year scenarios. The geological environment can have a significant impact on the formation of flash floods and thus on the resulting flood risk. The models also show that there is not necessarily a flood risk occurrence below all critical points, even during the 100-year scenario. In addition, it is still true that in the case of the Flysch zone, the so-called endangered area is significantly larger in our study areas, which is further evidence of the greater risk from floods in this geological area.

We suggest that methodologies used for the nationwide preliminary identification of "risk points" in terms of the occurrence of flash floods should also take into consideration significant differences in geological settings in the assessed areas. These differences in the geological setting may to some extent overestimate or underestimate the above-mentioned methodologies, which may ultimately introduce uncertainties into the preliminary flood risk assessment itself.

Our work has engendered a completely new finding regarding the hydrodynamic differences of flash floods in two different geological areas. We believe that these findings will help to refine the CPM method and possibly other similar methods as an even better tool in fighting flash floods, which are increasing phenomena in Europe (Kundzewicz et al., 2014). In the future, we would like to suggest a concrete way to achieve this. Additionally, we would like to further expand this topic, specifically by studying riverine floods. We want to examine the specifics of these floods in the Flysch zone and again compare them with those in the Bohemian Massif. Subsequently, we want to assess the impact that these differences may have, for example, on flood risk assessment, various revitalisations, flood control measures or other activities that are often applied based on national methodologies, without using different approaches to different geological environments. A more comprehensive analysis of the quantified differences in flood risk values in the different areas of the Flysch and Bohemian Massif could also be very interesting.

Acknowledgements

References:

ARCEMENT, G. J. (1989): Guide for Selecting Manning's Roughness Coefficients for Natural Channels and Flood Plains. United States Geological Survey: Water-Supply Paper 2339.

BAKY, M. A. A., ISLAM, M., PAUL, S. (2019): Flood Hazard, Vulnerability and Risk Assessment for Different Land Use Classes Using a Flow Model. Earth Systems and Environment, 4(1): 225–244.

BATES, P. D., HORRITT, M., HERVOUET, J. M. (1998): Investigating two-dimensional, finite element predictions of floodplain inundation using fractal generated topography. Hydrological Processes, 12(8): 1257–1277.

BAUGH, C. A., BATES, P. D., SCHUMANN, G., TRIGG, M. A. (2013): SRTM vegetation removal and hydrodynamic modelling accuracy. Water Resources Research, 49(9): 5276–5289.

BERKHAHN, S., FUCHS, L., NEUWEILER, I. (2019): An ensemble neural network model for real-time prediction of urban floods. Journal of Hydrology, 575: 743–754.

BEVEN, K. J. (2009): Environmental Modelling: An Uncertain Future?. Abingdon, Routledge.

BLADÉ, E. et al. (2014): Iber: herramienta de simulación numérica del flujo en ríos. Revista Internacional de Métodos Numéricos para Cálculo y Diseńo en Ingeniería, 30(1): 1–10.

BLÖSCHL, G. et al. (2020): Current European flood-rich period exceptional compared with past 500 years. Nature, 583: 560–566.

BODOQUE, J. M., AMERIGO, M., DIEZ-HERRERO, A., GARCIA, J. A., CORTES, B., BALLESTEROS-CANOVAS, J. A., OLCINA, J. (2016): Improvement of resilience of urban areas by integrating social perception in flash-flood risk management. Journal of Hydrology, 541: 665–676.

BONACCI, O., LJUBENKOV, I., ROJE-BONACCI, T. (2006): Karst flash floods: an example from the Dinaric karst (Croatia). Natural Hazards and Earth System Sciences, 6(2): 195–203.

BRATH, A., MONTANARI, A., MORETTI, G. (2006): Assessing the effect on flood frequency of land use change via hydrological simulation (with uncertainty). Journal of Hydrology, 324(1–4): 141–153.

BRUNNER, G. W. (2016): HEC-RES River Analysis System - User's Manual Version 5.0. US Army Corps of Engineers. Institute for Water Resources, Hydrologic Engineering Center (HEC).

BRYNDAL, T. (2015): Local flash floods in Central Europe: A case study of Poland. Norsk Geografisk Tidsskrift–Norwegian Journal of Geography, 69: 288–298.

CHEN, X., PARAJKA, J., SZÉLES, B., VALENT, P., VIGLIONE, A., BLÖSCHL, G. (2020): Impact of Climate and Geology on Event Runoff Characteristics at the Regional Scale. Water, 12(12): 3457.

CLUBB, F. J., MUDD, S. M., MILODOWSKI, D. T., VALTERS, D. A., SLATER, L. J., HURST, M. D., LIMAYE, A. B. (2017): Geomorphometric delineation of floodplains and terraces from objectively defined topographic thresholds. Earth Surface Dynamics, 5: 369–385.

ČUZK (n. d.): Digitální model reliéfu České republiky 5. generace (DMR 5G). URL: https://geoportal.cuzk.cz/(S(hg5uvv0eikuxv3c5pyise34q))/Default.aspx?mode=TextMeta&side=vyskopis&metadataID=CZ-CUZK-DMR5G-V&head_tab=sekce-02-gp&menu=302

COSTABILE, P., MACCHIONE, F., NATALE, L., PETACCIA, G. (2015): Flood mapping using LIDAR

DEM. Limitations of the 1-D modelling highlighted by the 2-D approach. Natural Hazards, 77(1): 181–204.

DIAKAKIS, M., DELIGIANNAKIS, G., ANDREADAKIS, E., KATSETSIADOU, K. N., SPYROU, N. I., GOGOU M. E. (2020): How different surrounding environments influence the characteristics of flash flood-mortality: The case of the 2017 extreme flood in Mandra, Greece. Journal of Flood Risk Management, 13(3): e12613.

DIEHL, T. H. (1997): Potential Drift Accumulation at Bridges. Department of Transportation, Federal Highway Administration Research and Development, TurnerFairbank Highway Research Center, Virginia. Publication No. FHWA-RD-97-028.

DINH, Q., BALICA, S., POPESCU, I., JONOSKI, A. (2012): Climate change impact on flood hazard, vulnerability and risk of the Long Xuyen Quadrangle in the Mekong Delta. International Journal of River Basin Management, 10(1): 103–120.

DRBAL, K. et al. (2009): Vyhodnocení povodní v červnu a červenci 2009 na území České republiky. Metodika mapování povodňového rizika: Dílčí zpráva. Praha, VÚV TGM, Ministerstvo životního prostředí.

DUB, O. (1957): Hydrológia, hydrografia, hydrometria. Slovenské vydavateľstvo technickej literatúry.

ERNST, J., DEWALS, B. J., DETREMBLEUR, S., ARCHAMBEAU, P., ERPICUM, S., PIROTTON, M. (2010): Micro-scale flood risk analysis based on detailed 2D hydraulic modelling and high resolution geographic data. Natural Hazards, 55(2): 181–209.

EUROPEAN COMMISSION (2006): Proposal for and Directive of the European Parliament and of the Council on the assessment and management of floods. Brussels, Commission of the European Communities.

EUROPEAN COMMISSION (2007): Directive 2007/60/EC of the European Parliament and of the Council of 23 October 2007 on the assessment and management of flood risks. European Parliament and Council. Official Journal of the European Union, L, 288: 27–34.

FILIPOVA, V., HAMMOND, A., LEEDAL, D., LAMB, R. (2022): Prediction of flood quantiles at ungauged catchments for the contiguous USA using Artificial Neural Networks. Hydrology Research, 53(1): 107–123.

FRAGOSO, M., TRIGO, R. M., PINTO, J. G., LOPES, S., LOPES, A., ULBRICH, S., MAGRO, C. (2012): The 20th February 2010 Madeira flash-floods: synoptic analysis and extreme rainfall assessment. Natural Hazards and Earth System Sciences, 12(3): 715–730.

GAÁL, L., SZOLGAY, J., KOHNOVÁ, S., PARAJKA, J., MERZ, R., VIGLIONE, A., BLÖSCHL, G. (2012): Flood timescales: Understanding the interplay of climate and catchment processes through comparative hydrology. Water Resources Research, 48(4): W04511.

GARROTE, J., ALVARENGA, F. M., DIEZ-HERRERO, A. (2016): Quantification of flash flood economic risk using ultra-detailed stage-damage functions and 2-D hydraulic models. Journal of Hydrology, 541: 611–625.

GAUME, E. et al. (2009): A compilation of data on European flash floods. Journal of Hydrology, 367(1–2): 70–78.

GRAY, D. M. (1964): Physiographic Characteristics and the Runoff Pattern. In: Proceedings of Hydrology

Symposium No. 4 (pp. 147–164). National Research Council of Canada.

GUTIÉRREZ, F., PARISE, M., DE WAELE, J., JOURDE, H. (2014): A review on natural and human-induced geohazards and impacts in karst. Earth-Science Reviews, 138: 61–88.

GVOŽDÍKOVÁ, B., MÜLLER, M. (2017): Evaluation of extensive floods in western/Central Europe. Hydrology and Earth System Sciences, 21(7): 3715–3725.

HANZE: Historical Analysis of Natural Hazards in Europe (2017): T. U. Delft, Faculty of Civil Engineering and Geosciences, Department of Hydraulic Engineering.

HAPUARACHCHI, H. A. P., WANG, Q. J., PAGANO, T. C. (2011): A review of advances in flash flood forecasting. Hydrological Processes, 25(18): 2771–2784.

HARDY, J., GOURLEY, J. J., KIRSTETTER, P. E., HONG, Y., KONG, F., FLAMIG, Z. L. (2016): A method for probabilistic flash flood forecasting. Journal of Hydrology, 541: 480–494.

HEWLETT, J. D., HIBBERT, A. R. (1967): Factors affecting the response of small watersheds to precipitation in humid areas. Forest hydrology, 1: 275–290.

HUISMAN, J. A. et al. (2009): Assessing the impact of land use change on hydrology by ensemble modelling (LUCHEM) III: Scenario analysis. Advances in Water Resources, 32(2): 159–170.

HYDRAULIC REFERENCE MANUAL IBER V. 1.0. (2014): Two-dimensional modelling of free surface shallow water flow.

JARIHANI, A. A., CALLOW, J. N., MCVICAR, T. R., VAN NIEL, T. G., LARSEN, J. R. (2015): Satellite-derived Digital Elevation Model (DEM) selection, preparation and correction for hydrodynamic modelling in large, low-gradient and data-sparse catchments. Journal of Hydrology, (524): 489–506.

KANDILIOTI, G., MAKROPOULOS, C. (2011): Preliminary flood risk assessment: the case of Athens. Natural Hazards. 61(2): 441–468.

KREIBICH, H., BUBECK, P., VLIET, M. V., MOEL, H. D. (2015): A review of damage-reducing measures to manage fluvial flood risks in a changing climate. Mitigation and Adaptation Strategies for Global Change, 20(6): 967–989.

KREIBICH, H., PIROTH, K., SEIFERT, I., MAIWALD, H., KUNERT, U., SCHWARZ, J., MERZ, B., THIEKEN, A. H. (2009): Is flow velocity a significant parameter in flood damage modelling? Natural Hazards and Earth System Sciences, 9(5): 1679–1692.

KRZHIZHANOVSKAYA, V. V. et al. (2011): Flood early warning system: design, implementation and computational modules. In: International Conference on Computational Science: Procedia Computer Science, 4: 106–115.

KOURGIALAS, N. N., KARATZAS, G. P. (2011): Flood management and a GIS modelling method to assess flood-hazard areas—a case study. Hydrological Sciences Journal, 56(2): 212–225.

KUKAL, Z. (2005): Geologická role řek v krajině. In: KENDER, J., POŠMOURNÝ, K., KUKAL, Z. [eds.]: Krajina v geologii – geologie v krajině (pp. 45–46). Praha, Ministerstvo životního prostředí ČR.

KUNDZEWICZ, Z. W. et al. (2014): Flood risk and climate change: global and regional perspectives. Hydrological Sciences Journal, 59(1): 1–28.

KUNDZEWICZ, Z. W., PIŃSKWAR, I., BRAKENRIDGE, G. R. (2018): Changes in river flood hazard in Europe: a review. Hydrology Research, 49(2): 294–302.

LAUBER, U., KOTYLA, P., MORCHE, D., GOLDSCHEIDER, N. (2014): Hydrogeology of an Alpine rockfall aquifer system and its role in flood attenuation and maintaining baseflow. Hydrology and Earth System Sciences, 18(11): 4437–4452.

LI, W., LIN, K., ZHAO. T., LAN, T., CHEN, X., DU, H., CHEN, H. (2019): Risk assessment and sensitivity analysis of flash floods in ungauged basins using coupled hydrologic and hydrodynamic models. Journal of Hydrology, 572: 108–120.

LI, Y., WANG C. (2009): Impacts of Urbanization on Surface Runoff of the Dardenne Creek Watershed, St. Charles County, Missouri. Physical Geography, 30: 556–573.

LI, K., WU, S., DAI, E., XU, Z. (2012): Flood loss analysis and quantitative risk assessment in China. Natural Hazards, 63(2): 737–760.

LIU, L. (2018): Application of a Hydrodynamic and Water Quality Model for Inland Surface Water Systems. In: Malcangio, D. [ed.]: Applications in Water Systems Management and Modeling.

MARCHI, L., BORGA, M., PRECISO, E., GAUME, E. (2010): Characterisation of selected extreme flash floods in Europe and implications for flood risk management. Journal of Hydrology, 394(1–2): 118–133.

MOSAVI, A., OZTURK, P., CHAU, K. (2018): Flood Prediction Using Machine Learning Models: Literature Review. Water, 10(11): 1536.

MASOOD, M., TAKEUCHI, K. (2012): Assessment of flood hazard, vulnerability and risk of mid-eastern Dhaka using DEM and 1D hydrodynamic model. Natural Hazards, 61(2): 757–770.

MARK, O., WEESAKUL, S., APIRUMANEKUL, C., AROONNET, S. B., DJORDJEVIĆ, S. (2004): Potential and limitations of 1D modelling of urban flooding. Journal of Hydrology, 299(3–4): 284–299.

MERZ, B., THIEKEN, A. H., GOCHT, M. (2007): Flood risk mapping at the local scale: concepts and challenges. In: Begum, S., Stive, M. J. F, Hall, J. W. [eds.]: Flood risk management in Europe, Springer, Berlin, pp. 231–251.

MIHU-PINTILIE, A., CIMPIANU, C. I, STOLERIU, C. C., PEREZ, M. N., PAVELUC, L. E.(2019): Using High-Density LiDAR Data and 2D Streamflow Hydraulic Modeling to Improve Urban Flood Hazard Maps: A HEC-RAS Multi-Scenario Approach. Water, 11(9): 1832.

MŁYŃSKI, D. (2020): Analysis of Problems Related to the Calculation of Flood Frequency Using Rainfall-Runoff Models: A Case Study in Poland. Sustainability, 12(17): 7187.

NOVÁK, P., TOMEK, M. (2015): Prevence a zmírňování následků přívalových povodní ve vztahu k působnosti obcí: metodika. Praha, Výzkumný ústav meliorací a ochrany půdy.

NEAL, J. C., FEWTRELL, T. J., BATES, P. D., WRIGHT, N. G. (2010): A comparison of three parallelisation

methods for 2D flood inundation models. Environmental Modelling & Software, 25(4): 398–411.

NTELEKOS, A. A., GEORGAKAKOS, K. P., KRAJEWSKI, W. F. (2006): On the Uncertainties of Flash Flood Guidance: Toward Probabilistic Forecasting of Flash Floods. Journal of Hydrometeorology, 7(5): 896–915.

NORBIATO, D., BORGA, M., MERZ, R., BLÖSCHL, G., CARTON, A. (2009): Controls on event runoff coefficients in the eastern Italian Alps. Journal of Hydrology, 375(3–4): 312–325.

O'CONNOR, J. E., GRANT, G. E., COSTA, J. E. (2002): The Geology and Geography of Floods. In: House, P. K., Webb, R. H., Baker, V. R. Levish, D. R. [eds.]: Ancient Floods, Modern Hazards: Principles and Applications of Paleoflood Hydrology, Volume 5. American Geophysical Union, pp. 359–385.

OPENSTREETMAP® (2019): Data file made by OpenStreetMap contributors [online] [cit. 28.08.2021]. Available at: https://planet.openstreetmap.org

PAIVA, R. C. D., BUARQUE, D. C., COLLISCHONN, W., BONNET, M. P., FRAPPART, F., CALMANT, S., MENDES, C. A. B. (2013): Large-scale hydrologic and hydrodynamic modeling of the Amazon River basin, Water Resources Research, 49(3): 1226–1243.

PAPAIOANNOU, G., LOUKAS, A., VASILIADES, L., ARONICA, G. T. (2016): Flood inundation mapping sensitivity to riverine spatial resolution and modelling approach. Natural Hazards, 83(1): 117–132.

PAPPENBERGER, F., MATGEN, P., BEVEN, K. J., HENRY, J. B., PFISTER, L., DE FRAIPONT, P. (2006): Influence of uncertain boundary conditions and model structure on flood inundation predictions. Advances in Water Resources, 29(10): 1430–1449.

PAPROTNY, D., SEBASTIAN, A., MORALES-NÁPOLES, O., JONKMAN, S. N. (2018): Trends in flood losses in Europe over the past 150 years. Nature Communications, 9(1): 1–12.

PATEL, D. P., RAMIREZ, J. A., SRIVASTAVA, P. K., BRAY, M., HAN, D. (2017): Assessment of flood inundation mapping of Surat city by coupled 1D/2D hydrodynamic modeling: a case application of the new HEC-RAS 5. Natural Hazards, , 89(1): 93–130.

PESTANA, R. et al. (2013): Calibration of 2D hydraulic inundation model in the floodplain region of the lower Tagus River. Conference paper: ESA Living Planet Symposium.

PETROSELLI, A., VOJTEK, M., VOJTEKOVÁ, J. (2019): Flood mapping in small ungauged basins: a comparison of different approaches for two case studies in Slovakia. Hydrology Research, 50(1): 379–392.

PINOS, J., TIMBE L. (2019): Performance assessment of two-dimensional hydraulic models for generation of flood inundation maps in mountain river basins. Water Science and Engineering, 12(1): 11–18.

POUSSIN, J. K., BOTZEN, W. J. W., AERTS, J. C. J. H. (2015): Effectiveness of flood damage mitigation measures: Empirical evidence from French flood disasters. Global Environmental Change, 31: 74–84.

RUIZ-VILLANUEVA, V., BODOQUE, J. M., DÍEZ-HERRERO, A., EGUIBAR, M. A., PARDO-IGÚZQUIZA, E. (2012): Reconstruction of a flash flood with large wood transport and its influence on hazard patterns in an ungauged mountain basin. Hydrological Processes, 27(24): 3424–3437.

RUIZ-VILLANUEVA, V., CASTELLET, E. B., DÍEZ-HERRERO, A., BODOQUE, J. M., SÁNCHEZ-JUNY, M. (2014a): Two-dimensional modelling of large wood transport during flash floods. Earth Surface Processes and Landforms, 39(4): 438–449.

RUIZ-VILLANUEVA, V., BODOQUE, J. M., DÍEZ-HERRERO, A., BLADÉ, E. (2014b): Large wood transport as significant influence on flood risk in a mountain village. Natural Hazards, 74(2): 967–987.

RUMAN, S., BALL, T., BLACK, A. R., THOMPSON, J. R. (2020): Influence of alternative representations of land use and geology on distributed hydrological modelling results: Eddleston, Scotland. Hydrological Sciences Journal, 66(3): 488–502.

RUMAN, S., TICHAVSKÝ, R., ŠILHÁN, K., GRILLAKIS, M. G. (2021): Palaeoflood discharge estimation using dendrogeomorphic methods, rainfall-runoff and hydraulic modelling-a case study from southern Crete. Natural Hazards, 105(2): 1721–1742.

SCHUBERT, J. E., SANDERS, B. F. (2012): Building treatments for urban flood inundation models and implications for predictive skill and modeling efficiency. Advances in Water Resources, 41: 49–64.

SCHUMM, S. A. (1960): The shape of alluvial channels in relation to sediment type. Washington, USGS.

SCHUMM, S. A. (1985): Patterns of Alluvial Rivers. Annual Review of Earth and Planetary Sciences, 13: 5–27.

SENE, K. (2013): Flash Floods: Forecasting and Warning. Springer.

SEYOUM, S. D., VOJINOVIC, Z., PRICE, R. K., WEESAKUL, W. (2012): Coupled 1D and Noninertia 2D Flood Inundation Model for Simulation of Urban Flooding. Journal of Hydraulic Engineering, 138(1): 23–24.

SHARMA, P. J., PATEL, P., JOTHIPRAKASH, V. (2019): Assessment of variability in runoff coefficients and their linkages with physiographic and climatic characteristics of two contrasting catchments. Journal of Water and Climate Change, 10(3): 464–483.

SMITH, D. I. (1994): Flood damage estimation – A review of urban stage-damage curves and loss functions. Water Sa, 20(3): 231–238.

SMOLDERS, S., IDES, S., PLANCKE, Y., MEIRE, P., TEMMERMAN, S. (2012): Calibrating discharges in a 2D hydrodynamic model of the Scheldt Estuary: Which parameters can be used and what is their sensitivity. In: Proceeedings of the 10th International Conference on Hydroinformatics (pp. 14–18). Hambrug, Germany.

SPELLMAN, P., GULLEY, J., MARTIN, J. B., LOUCKS, J. (2019): The role of antecedent groundwater heads in controlling transient aquifer storage and flood peak attenuation in karst watersheds. Earth Surface Processes and Landforms, 44(1): 77–87.

SRINIVAS, K., WERNER, M., WRIGHT, N. (2009): Comparing forecast skill of inundation models of differing complexity: the case of Upton upon Severn. London, Taylor & Francis Group.

ŠTĚPÁNKOVÁ, P., DUMBROVSKÝ, M., DRBAL, K. (2017): The Assessment of Level of Flash Floods Threat of Urbanised Areas. Acta Universitatis Agriculturae et Silviculturae Mendelianae Brunensis, 65(2): 519–526.

SUBRAMANYA, K. (2008): Engineering Hydrology. 3rd edition. New Dehli, Tata McGraw-Hill Publishing Company Ltd.

TENG, J., JAKEMAN, A. J., VAZE, J., CROKE, B. F. W., DUTTA, D., KIM, S. (2017): Flood inundation modelling: A review of methods, recent advances and uncertainty analysis. Environmental Modelling & Software, 90: 201–216.

TRPKOSOVA, D., KRASNY, J., PAVLIKOVA, D. (2008): Differences in runoff conditions of crystalline and flysh regions in Moravia and Silesia. Journal of Hydrology and Hydromechanics, 56(3): 201–210.

UNDRR (2019): Global Assessment Report on Disaster Risk Reduction. Geneva, Switzerland, United Nations Office for Disaster Risk Reduction.

VAN ALPHEN, J., MARTINI, F., LOAT, R., SLOMP, R., PASSCHIER, R. (2009): Flood risk mapping in Europe, experiences and best practices. Journal of Flood Risk Management, 2(4): 285–292.

VAZE, J., TENG, J., SPENCER, G. (2010): Impact of DEM accuracy and resolution on topographic indices. Environmental Modelling & Software, 25(10): 1086–1098.

VINCENDON, B., DUCROCQ, V., NUISSIER, O., VIÉ, B. (2011): Perturbation of convection-permitting NWP forecasts for flash-flood ensemble forecasting. Natural Hazards and Earth System Sciences, 11(5): 1529–1544.

VOJTEK, M., PETROSELLI, A., VOJTEKOVÁ, J., ASGHARINIA, S. (2019): Flood inundation mapping in small and ungauged basins: sensitivity analysis using the EBA4SUB and HEC-RAS modeling approach. Hydrology Research, 50(4): 1002–1019.

VOJTEK, M., VOJTEKOVÁ, J. (2016): Flood hazard and flood risk assessment at the local spatial scale: a case study. Geomatics, Natural Hazards and Risk, 7(6): 1973–1992.

WANG, Y., LI, Z., TANG, Z., ZENG, G. (2011): A GIS-Based Spatial Multi-Criteria Approach for Flood Risk Assessment in the Dongting Lake Region, Hunan, Central China. Water Resources Management, 25(13): 3465–3484.

WINSEMIUS, H. C. et al. (2016): Global drivers of future river flood risk. Nature Climate Change, 6(4): 381–385.

WISNER, B., BLAIKIE, P, CANNON, T., DAVIS, I. (2004): At Risk: Natural Hazards, People's Vulnerability and Disasters. Routledge.

XIA, X., LIANG, Q., MING, X. (2019): A full-scale fluvial flood modelling framework based on a high-performance integrated hydrodynamic modelling system (HiPIMS). Advances in Water Resources, 132: 103392.

ZANCHETTA, A. D. L., COULIBALY, P. (2020): Recent Advances in Real-Time Pluvial Flash Flood Forecasting. Water, 12(2): 1–29.

ZANON, F. et al. (2010): Hydrological analysis of a flash flood across a climatic and geologic gradient: The September 18, 2007 event in Western Slovenia. Journal of Hydrology, 394(1–2): 182–197.

ZELEŇÁKOVÁ, M., GAŇOVÁ, L., PURCZ, P, SATRAPA, L. (2015): Methodology of flood risk assessment from flash floods based on hazard and vulnerability of the river basin. Natural Hazards, 79(3): 2055–2071.